Chinese Chemical Letters 34 (2023) 107365

Contents lists available at ScienceDirect

Chinese Chemical Letters

journal homepage: www.elsevier.com/locate/cclet

Ni_4-thiacalix[4]arene sandwiched Mo_8 polyoxometalate bimetallic nanoclusters for electrocatalytic glucose oxidation

Meilin Wang, Yinjuan Guo, Guiyan Zhao, Baokuan Chen, Yanfeng Bi*

School of Petrochemical Engineering, Liaoning Petrochemical University, Fushun 113001, China

ARTICLE INFO

Article history:
Received 9 March 2022
Revised 20 March 2022
Accepted 21 March 2022
Available online 24 March 2022

Keywords:
Thiacalix[4]arene
Substituted polyoxometalates
Bimetallic nanocluster
Crystal structure
Glucose oxidation

ABSTRACT

Available online two new Ni_8Mo_8 bimetallic coordination clusters, $[Ni_4(TC4A)]_2[(Mo_5^{V}Mo_3^{VI}O_{24})(PO_4)]$ (+Solvent) (Ni_8PMo_8, H_4TC4A= *p-tert*-butylthiacalix[4]arene) and $[Ni_4(TC4A)]_2[(Mo_5^{V}Mo_3^{VI}O_{24})(OH)(CO_3)]$ (+Solvent) (Ni_8Mo_8), were synthesized by solvothermal method and structurally characterized by single-crystal X-ray diffraction, powder X-ray diffraction, FT-IR spectroscopy, and TGA experiments, respectively. The usage of $H_3PMo_{12}O_{40}$ as source for Ni_8PMo_8 resulted a sandwich like structure built from two Ni_4-thiacalix[4]arene units and a Mo_8 polyoxometalate with inner spaces of PO_4^{3-}. Ni_8Mo_8 with the similar structure to that of Ni_8PMo_8 is from H_2MoO_4 starting reagent with OH^- and CO_3^{2-} anions encapsulated in the center. The two clusters can be directly loaded on carbon paper and utilized as working electrodes which showed distinguishable performances for glucose detection and oxidation. This work provides a better understanding of the structure–property relationships in using substituted polyoxometalates for electrochemical applications and is helpful for building calixarene-based or polyoxometalate-based functional materials.

Polyoxometalates (POMs) are a class of metal-oxygen cluster compounds composed of pre-transition metals, such as Mo^{V}, Mo^{VI}, W^{VI}, V^{V}, Nb^{V} and Ta^{V}, by shared oxygen atoms [1,2]. Due to the ample of redox electron pairs, pure POMs are sensitive to stimulation [3,4]. In recent decade, a great number of metal-substituted POMs [5], pure organic-ligands sheeted POMs [6], hybrid organic-inorganic POMs compounds [7], and POM-based metal-organic frameworks [8,9] have been widely investigated to regulate the physical and chemical performances. Among them, the direct modification of organic ligands on POMs can not only improve the stability under specific conditions but also tune the electronic structures while the strategy is limited by a finite number of atoms that can be utilized to coordinate [6]. The introduction of metal ions for coordination to bridge POMs and organic ligands has been proved to be a feasible way for functionalized POMs [5,10].

Thiacalixarene, a cyclic phenol tetramer bridged by sulfur atoms, is an ideal multidentate ligand for building nanoclusters [11–13]. Thiacalix[4]arene generally bond metals to form a shuttlecock-like polynuclear secondary building unit (PSBU), which can be served for modular construction for various nanoclusters [14–16]. Thiacalix[4]arene-based nanoclusters have received exceptional attention due to their magnetic [17], catalytic [18], electrochemical properties [19], and molecular recognition [20]. As a result of the π-rich cavity and strong inclusion properties, calixarene and their derivatives can be used as hosts to include guests through intermolecular interactions to form host-guest complexes [21,22]. The modification POMs with calixarenes is beneficial for fabricating functional hybrid materials with combined merits of the two components [23,24]. Very recently, we successfully combined a sulfur-modified Mo_8 with a Co_4-thiacalix[4] arene unit to produce a bimetallic Co_4Mo_8 electrocatalyst, which showed Co-Mo synergy effect and durability for electrocatalytic water oxidation [25]. However, the research on thiacalix[4]arene-based molybdenum containing nanoclusters is still in the infancy and it is also challenging for synthesizing such complexes [24–28].

As our continuous on thiacalix[4]arene supported functional nanoclusters, here we report two nickel-thiacalix[4]arene modified POM-based bimetallic coordination clusters: $[Ni_4(TC4A)]_2[(Mo_5^{V}Mo_3^{VI}O_{24})(PO_4)]$ (+Solvent) (Ni_8PMo_8) and $[Ni_4(TC4A)]_2[(Mo_5^{V}Mo_3^{VI}O_{24})(OH)(CO_3)]$ (+Solvent) (Ni_8Mo_8) (H_4TC4A = *p-tert*-butylthiacalix[4]arene). The specific details of the syntheses, characterizations, and structure analyses for two clusters and the electrochemical detection and electrocatalytic oxidation for glucose have been provided (Some detailed information of this work was supplied in Supporting information.).

Single–crystal X–ray diffraction demonstrated that both Ni_8PMo_8 and Ni_8Mo_8 crystallize in the monoclinic system with

* Corresponding author.
E-mail address: biyanfeng@lnpu.edu.cn (Y. Bi).

https://doi.org/10.1016/j.cclet.2022.03.088
1001-8417/

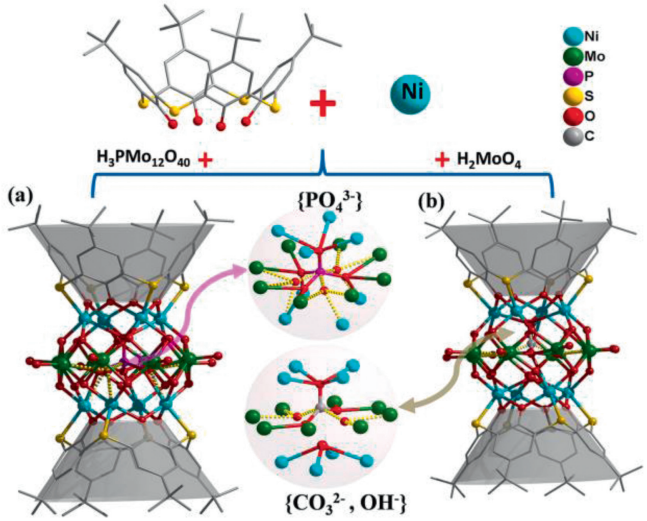

Fig. 1. Schematic illustration of the synthesis of (a) Ni_8PMo_8 and (b) Ni_8Mo_8.

the space group $P2_1/m$ (Table S1 in Supporting information). As shown in Fig. 1, Ni_8PMo_8 cluster can be regarded as a sandwich structure composed of two tail-to-tail shuttlecock-like Ni_4-TC4A secondary building units (SBUs) in-between one $\{Mo_8O_{24}\}(Mo_8)$ unit. The Mo_8 unit in Ni_8PMo_8 can be viewed as a ring of eight Mo atoms from the decomposion and re-selfassembly of $H_3PMo_{12}O_{40}$ (PMo_{12}). The inner space of Ni_8PMo_8 located disordered $\{PO_4\}$ units which is also from PMo_{12} source (Fig. 1a). Since PMo_{12} can be decomposed and utilized as Mo sources, we are curious what structure we will get by directly using H_2MoO_4. Under equivalent synthesis conditions, the replacement of PMo_{12} with H_2MoO_4 resulted a Ni_8Mo_8 cluster with the similar framework to that of Ni_8PMo_8. However, in inner cavity of Ni_8Mo_8 coordinated with OH^- and CO_3^{2-} anions. The OH^- bonded to the bottom of one Ni_4-TC4A SBU while CO_3^{2-} is close to another SBU (Fig. 1b). CO_3^{2-} may be derived from CO_2 in air, since prolonged exposure of the starting mixture for Ni_8Mo_8 under ambient prior to solvothermal reaction can significantly increase crystal yield. All the Ni centers in two nanoclusters are six-coordinated with two μ_2-O oxygen atoms from phenol, two μ_3-O atoms sharing with Mo, one sulfur atom from TC4A and one oxygen from the inner units. The Mo coordination enviroment is complicated in both two nanoclusters. By splitting disordered modes for $\{PO_4\}$ and CO_3^{2-} units based on symmetry operation, one can find the Mo centers for two nanoclusters is also six-coordinated in general. The five coordiates (four bridging μ_3-O and one terminal O) are in normal environment as that in popular POM [3] and the six one is from the disordered inner units. The $\{PO_4\}$ units bridge eight Mo centers *via* two pairs (each for three) of disordered μ_3-O atoms while CO_3^{2-} anion connected eight Mo by two pairs (each for two) of disordered μ_2-O. The splited μ_3-O atoms from $\{PO_4\}$ in Ni_8PMo_8 bond with two Mo and one Ni centers. The μ_4-O with normal location in $\{PO_4\}$ and CO_3^{2-} units coordinate with four Ni in a Ni_4-TC4A SBU simultaneously, respectively. The average nearest Ni–Mo distances bridged by two μ_3-O on the surface of Mo_8 units is 3.025 Å and 3.096 Å for Ni_8PMo_8 and Ni_8Mo_8, respectively. The combination of the bond valance calculations, the bonding modes analysis, and the overall charge banlance consideration indicate the bivalence of Ni cations, mixture valence for Mo (five for V and three for VI) in two nanoclusters and pentavalence for P in Ni_8PMo_8 (Table S2 in Supporting information). The partially reduction of Mo from VI in feeding materials to V in the products might caused by thiacalixarene ligand and methanol solvent under solvothermal condition, which is also observed in literatures

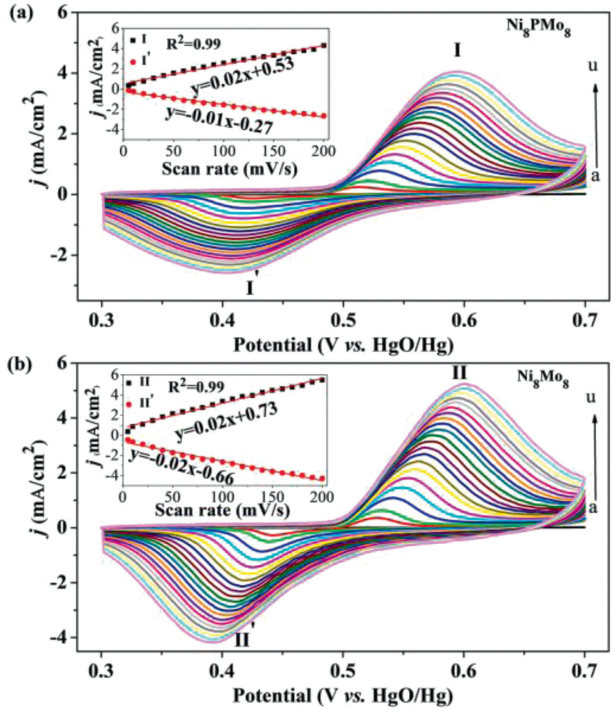

Fig. 2. Cyclic voltammograms of (a) Ni_8PMo_8-CP and (b) Ni_8Mo_8-CP in the 0.1 mol/L KOH at different scan rates (a→u: bare CP, 5–200 mV/s). Insert: the linear dependence of anodic peak (I, II) and cathodic peak (I', II') current on scan rates.

[10,25,29]. The disordered solvent molecules filled in the crystal interstices have been subtracted by SQUEEZE during structure refinement (Fig. S1 in Supporting information). The two clusters have also been characteried by PXRD, FT-IR and TGA. PXRD indicate the purity of the bulk samples (Fig. S2 in Supporting information) and TGA showed both frameworks of two clusters are stable up to *ca.* 180 °C in N_2 media (Fig. S3 in Supporting information). FT-IR spectra showed characteristic C–H vibration *p-tert*-butyl groups and phenolic groups of calixarene (Fig S4 in Supporting information).

In POM chemistry, some classical examples has shown that the inner units encapsulated by poly-molybdenum can cause significant difference catalytic performances [5,29]. Both Ni_8PMo_8 and Ni_8Mo_8 clusters contain a Mo_8 ring, but the components wrapped in the center are completely different. The difference prompted us to study the electrochemical behavior of two metal clusters. Moreover, recent reports have also suggested the possibility of POM-based materials for glucose detection [30,31]. Furthermore, we also found that metal-thiacalixarene cluster might be a good catalyst as the abundant M-S bonds that can facilitate electron transfer in catalytic reactions [25,32].

Based on above considerations, the electrochemical performances and electrocatalytic activities for glucose oxidation (G-oxidation) of two clusters were investigated, respectively. Working electrodes were prepared by dissolving the two clusters in CH_2Cl_2 and then directly coating on carbon paper (CP), denoted as Ni_8PMo_8-CP and Ni_8Mo_8-CP. The cyclic voltammetry (CV) of two clusters in 0.1 mol/L KOH at different scan rates is depicted in Fig. 2. A pair of redox peaks located at 0.519 V (I), 0.423 V (I') for Ni_8PMo_8-CP and 0.532 V (II), 0.436 V (II') for Ni_8Mo_8-CP (scan rate: 10 mV/s; potentials *vs.* HgO/Hg reference electrode, the same afterwards) were observed, respectively, which can be assigned to the redox process of Ni^{II}/Ni^{III} [33,34]. It is noteworthy that although the two working electrodes presented linear surface-controlled plots and similar peak differences (<5 mV), both the an-

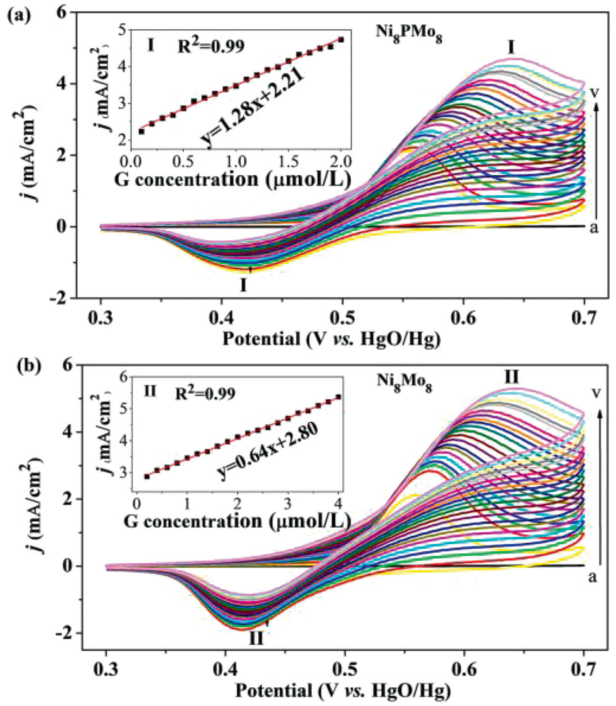

Fig. 3. Cyclic voltammograms of (a) Ni_8PMo_8-CP and (b) Ni_8Mo_8-CP in the 0.1 mol/L KOH with 0.1–2 μmol/L glucose and 0.2–4 μmol/L glucose concentrations. Scan rate: 50 mV/s. Insert: the linear dependence of anodic peak (I, II) on glucose concentration.

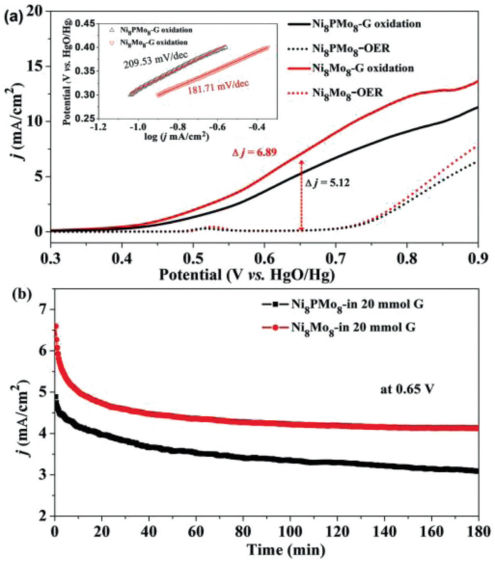

Fig. 4. (a) Comparison of LSVs in absent of glucose or containing 20 mmol/L glucose and (b) chronoamperometric response for Ni_8PMo_8-CP and Ni_8Mo_8-CP measured in 0.1 mol/L KOH. Insert in (a): corresponding Tafel plots.

odic peak (i_{pa}) and cathodic peak (i_{pc}) intensity of Ni_8Mo_8-CP is obviously higher than that of Ni_8PMo_8-CP under a same scan rate. The observations indicated the inner different components of the clusters, PO_4^{3-} for Ni_8PMo_8 and OH^- and CO_3^{2-} for Ni_8Mo_8, are responsible for the different electrochemical performances.

In the case of low glucose concentration, compared with that of without glucose, the i_{pa} in CVs linearly increased and moved in the direction of high potential for both electrodes (Fig. 3). The significantly elevated i_{pa} intensity and less variation of i_{pc} indicate the electrochemical G-oxidation by Ni^{III} [33,34]. G-concentration *vs.* current density (j) were well fitted (correlation coefficient: 0.99) as linear plots with slopes being 1.28 and 0.64 in the 0.1–2 μmol/L and 0.2–4 μmol/L ranges for Ni_8PMo_8-CP and Ni_8Mo_8-CP, respectively. The smaller slope and the wide detecting G-concentration ranges for Ni_8Mo_8-CP indicated the superior oxidation capacity than that of Ni_8PMo_8-CP. The sensitivity and limit of detection are 1.28 mA L μmol^{-1} cm^{-2} and 0.04 μmol/L, 0.64 mA L μmol^{-1} cm^{-2} and 0.03 μmol/L for Ni_8PMo_8-CP and Ni_8Mo_8-CP, respectively. The glucose detection performances two clusters are comparable or better than some Ni-based electrochemical sensor materials (Table S3 in Supporting information).

Linear sweep voltammetry (LSV, scan rate: 5 mV/s) also was applied to investigate the electrocatalytic activities for two electrodes for G-oxidation (Fig. S5 in Supporting information). After the glucose detection was completed, the current intensity in LSV curves gradually increased with the continuous addition of glucose. The total glucose consumption of Ni_8Mo_8-CP was *ca.* 8 μmol/L at 0.65 V before the current density remained unchanged after two successive addition operations, which is about 1.5 times than Ni_8PMo_8-CP (5.4 μmol/L). The G-concentration *vs.* Δj (comparing with in the absence of glucose) were fitted as linear dependent plots with slopes being 1.32 and 1.91 for Ni_8Mo_8-CP and Ni_8Mo_8-CP, respectively, which indicates the better capacity of the former electrode for G-oxidation.

Oxygen evolution reaction (OER) is the main competing reaction for G-oxidation [35]. The LSV profiles of the G-oxidation and OER for Ni_8PMo_8-CP and Ni_8Mo_8-CP electrodes in 0.1 mol/L KOH solution with 20 mmol/L glucose are presented in Fig. 4a. The addition of glucose significantly lowered the electrode initial overpotential from *ca.* 0.7 V (OER) to 0.3 V (G-oxidation) for electrocatalytic oxidation reaction. The Tafel slopes for G-oxidation estimated be 181.71 and 209.53 mV/dec (0.3–0.4 V) for Ni_8PMo_8-CP and Ni_8Mo_8-CP, respectively. There is almost no current density for OER at 0.65 V. Comparingly, Ni_8Mo_8-CP presented a current density of 6.89 mA/cm^2 at same potential for G-oxidation, which is higher than that of Ni_8PMo_8-CP (5.12 mA/cm^2). The long-term G-oxidation were carried out at a constant potential of 0.65 V by the chronoamperometric measurements (Fig. 4b). The current density decreased dramatically for Ni_8Mo_8-CP and reached to a relative constant j volume in about 3 h. In the same electrocatalytic G-oxidation time, the current density of Ni_8PMo_8-CP decreases slowly compared with that of Ni_8Mo_8-CP. Additionally, the smaller charge-transfer resistance (R_{ct}) of the Ni_8Mo_8-CP electrode in contrast to Ni_8PMo_8-CP also revealed the favourable electron transport rate and catalytic kinetics (Fig. S6 in Supporting information) [35].

To figure out how the inner components influence the electrocatalytic performances for G-oxidation, the rinsed and re-polished (renewed) electrodes were further investigated by CVs. Both of the renewed electrodes showed that the anode reaction ($Ni^{II} \rightarrow Ni^{III}$) current density increased and the anodic peaks moved to high potential comparing to the initial electrodes at a scan rate 50 mV/s (Fig. S7 in Supporting information). Obvious redox pairs with equal peak difference of 84 mV besides to Ni^{II}-Ni^{III} were observed for both renewed electrodes at a low scan rate of 1 mV/s, which can be assign to the $Mo^{V} \rightarrow Mo^{VI}$ (Fig. S8 in Supporting information). The corresponding peak differences for Ni^{II}/Ni^{III} redox pairs is 104 mV and 120 mV for renewed Ni_8Mo_8-CP and Ni_8PMo_8-CP electrodes, respectively. It is reasonable that the presence of Mo^{V}/Mo^{VI} significantly lowered the peak difference of the active $Ni^{II} \rightarrow Ni^{III}$ in Ni_8Mo_8-CP than that for Ni_8PMo_8-CP. The smaller peak difference indicated the faster and reversible redox processes for Ni_8Mo_8-CP than that for Ni_8PMo_8-CP, which might afford the former better electrocatalytic performances. Further LSV experiments on renewed electrodes indicated the recyclability for electrodes except

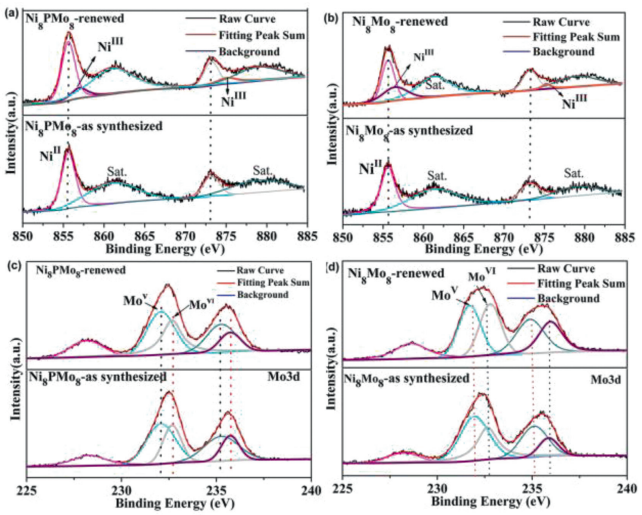

Fig. 5. High-resolution Ni 2p and Mo 3d XPS of (a) as-synthesized Ni_8PMo_8, (b) Ni_8Mo_8 and (c, d) after glucose oxidation.

for some changes that accordance with the CV investigations discussed above (Fig. S9 in Supporting information).

X-ray photoelectron spectrum (XPS) was used to probe the chemical environments of the as-synthesized crystals and renewed samples. Ni_8PMo_8 and Ni_8Mo_8 crystals showed almost identical chemical environments for Ni 2p and Mo 3d (Fig. S10 in Supporting information). The well fitted Ni_{2p} high-resolution spectra with peak positions at 855.59 and 873.23 eV indicated the presence of Ni^{II} for both crystal clusters [34,36]. The high-resolution of spectra Mo 3d for crystal samples divided into two pairs fitted peaks at 232.06 eV and 234.8 eV, 232.6 eV and 235.7 eV, which could be attributed to Mo^{V} and Mo^{VI}, respectively [25]. The calculated Mo^{VI} and Mo^{V} ratios are all close to 3:5, which is accordance to that found in the crystal structure refinement (Table S4 in Supporting information). Generally, one metal center response for active site to facilitate the electron transfer of electrolytes while another one can tune the intrinsic catalytic performances in a bimetallic electrocatalyst [25]. Both Ni^{III} signal and increasement of Mo^{VI} ratio were observed for the renewed samples (Fig. 5). The Ni^{III}/Ni^{II} and Mo^{VI}/Mo^{V} ratio estimated to be 0.33 and 0.70 for Ni_8PMo_8 and 0.61 and 0.90 for Ni_8Mo_8, respectively, which indicated the interacted synergistic effect between Ni and Mo. The presence of both larger Ni^{III}/Ni^{II} and Mo^{VI}/Mo^{V} ratios for Ni_8Mo_8 indicated the superior oxidation capacity than that of Ni_8PMo_8. The above discussions indicate that the electrocatalytic glucose oxidation mainly originated from Ni^{II}/Ni^{III} redox active sites and tuned by Mo^{V}/Mo^{VI} sites.

Additionally, the high-resolution spectra for C 1s, O 1s and S 2p kept almost unchanged before and after glucose oxidation (Fig. S11 in Supporting information). Furthermore, no Ni or Mo element signal was detected in the electrolytes after long-term oxidation by ICP-AES analysis. Moreover, the EDS mapping for the samples after oxidation experiments show the well overlapped elements in the same area (Figs. S12 and S13 in Supporting information). All these results proved the stability of the cluster frameworks after reaction.

In summary, we have successfully synthesized and characterized two bimetallic coordination clusters Ni_8PMo_8 and Ni_8Mo_8. The framework of the two clusters is built from a polymolybdenum Mo_8 sandwiched by two Ni_4-thiacalxiarene units. The inner cavity of two clusters incorporated different components, PO_4^{3-} for Ni_8PMo_8 and OH^- and CO_3^{2-} for Ni_8Mo_8, which resulted from the different Mo feed sources. The same exterior structure while different interior "chips" of the two clusters afforded the prepared binder free and active carbon free electrodes with distinguishable electrochemical sensing and electrocatalytic performances for glucose. The synergistic effect of Ni-Mo is identified experimentally and the superior effect for Ni_8Mo_8 than that for Ni_8PMo_8 can be attributed to the weak coordination of OH^- and CO_3^{2-} in the former core, and the strong coordination of PO_4^{3-} in the latter. Our work combines polyoxometalate and calixarene merits to prepare two bimetallic clusters, providing an example for studying the structure-activity relationship.

Declaration of competing interest

The authors declare that they have no known competing financial interests or personal relationships that could have appeared to influence the work reported in this paper.

Acknowledgment

This work was supported by the National Natural Science Foundation of China (No. 91961110).

Supplementary materials

Supplementary material associated with this article can be found, in the online version, at doi:10.1016/j.cclet.2022.03.088.

References

[1] D.L. Long, R. Tsunashima, L. Cronin, Angew. Chem. Int. Ed. 49 (2010) 1736–1758.
[2] M.T. Pope, A. Müller, Angew. Chem. Int. Ed. 30 (1991) 34–48.
[3] M. Sadakane, E. Steckhan, Chem. Rev. 98 (1998) 219–237.
[4] T. Yamase, M.T. Pope, Polyoxometalate Chemistry for Nanocomposite Design, Kluwer, Dordrecht, 2002.
[5] D.D. Li, P.T. Ma, J.Y. Niu, J.P. Wang, Coord. Chem. Rev. 392 (2019) 49–80.
[6] J.W. Zhang, Y.C. Huang, G. Li, Y.G. Wei, Coord. Chem. Rev. 378 (2019) 395–414.
[7] A. Dolbecq, E. Dumas, C.R. Mayer, P. Mialane, Chem. Rev. 110 (2010) 6009–6048.
[8] L. Vilà-Nadal, L. Cronin, Nat. Rev. Mater. 2 (2017) 17054–17068.
[9] J.X. Liu, X.B. Zhang, Y.L. Li, S.L. Huang, G.Y. Yang, Coord. Chem. Rev. 414 (2020) 213260.
[10] Y. Zhang, J. Liu, S.L. Li, Z.M. Su, Y.Q. Lan, J. Energy Chem. 1 (2019) 100021–100078.
[11] N. Morohashi, F. Narumi, N. Iki, T. Hattori, S. Miyano, Chem. Rev. 106 (2006) 5291–5316.
[12] R. Kumar, Y.O. Lee, V. Bhalla, M. Kumar, J.S. Kim, Chem. Soc. Rev. 43 (2014) 4824–4870.
[13] A. Ovsyannikov, S. Solovieva, I. Antipin, S. Ferlay, Coord. Chem. Rev. 352 (2017) 151–186.
[14] T. Kajiwara, N. Iki, M. Yamashita, Coord. Chem. Rev. 251 (2007) 1734–1746.
[15] Y.F. Bi, S.C. Du, W.P. Liao, Coord. Chem. Rev. 276 (2014) 61–72.
[16] H.T. Han, L. Kan, P. Li, et al., Sci. China Chem. 64 (2021) 426–431.
[17] R.O. Fuller, G.A. Koutsantonis, M.I. Ogden, Coord. Chem. Rev. 402 (2020) 213066–213082.
[18] X.X. Hang, Y.F. Bi, Dalton Trans. 50 (2021) 3749–3758.
[19] C.J. Mei, S.A.A. Ahmad, Arab. J. Chem. 14 (2021) 103303–103340.
[20] M. Yamada, M.R. Gandhi, U.M.R. Kunda, F. Hamada, J. Incl. Phenom. Macrocycl. Chem. 85 (2016) 1–18.
[21] Y. Ishii, Y. Takenaka, K. Konishi, Angew. Chem. Int. Ed. 43 (2004) 2702–2705.
[22] Y. Ishii, N. Nakayama, K. Konishi, Chem. Lett. 36 (2007) 246–247.
[23] C. Aronica, G. Chastanet, E. Zueva, et al., J. Am. Chem. Soc. 130 (2008) 2365–2371.
[24] Y.F. Bi, S.C. Du, W.P. Liao, Chem. Commun. 47 (2011) 4724–4726.
[25] M. Zhang, M.W. Chen, Y.F. Bi, et al., J. Mater. Chem. A 7 (2019) 12893–12899.
[26] X.X. Hang, Y.N. Yu, Z. Wang, Y.F. Bi, Cryst. Growth Des. 20 (2020) 7934–7940.
[27] D. Buccella, G. Parkin, J. Am. Chem. Soc. 130 (2008) 8617–8619.
[28] D. Buccella, G. Parkin, Chem. Commun. (2009) 289–291.
[29] X.B. Han, Z.M. Zhang, T. Zhang, et al., J. Am. Chem. Soc. 136 (2014) 5359–5366.
[30] S. Liu, J.Q. Tian, L. Wang, et al., ChemPlusChem 77 (2012) 541–544.
[31] R. Ayranci, Y. Torlak, M. Ak, J. Electrochem. Soc. 166 (2019) B205–B211.
[32] X. Wang, Y.N. Yu, Z. Wang, et al., Inorg. Chem. 59 (2020) 7150–7157.
[33] S.T. Wang, X.H. Gao, X.X. Hang, et al., J. Am. Chem. Soc. 140 (2018) 6271–6277.
[34] K.K. Naik, S. Ratha, C.S. Rout, ChemistrySelect 1 (2016) 5187–5195.
[35] W.J. Liu, Z.R. Xu, D.T. Zhao, et al., Nat. Commun. 11 (2020) 265–275.
[36] D.H. Yang, Y.F. Liang, P.T. Ma, et al., CrystEngComm 16 (2014) 8041–8046.